

# Theoretical study of finite temperature spectroscopy in van der Waals clusters. II

## Time-dependent absorption spectra

F. Calvo, F. Spiegelman

*Laboratoire de Physique Quantique, IRSAMC, Université Paul Sabatier,  
118 Route de Narbonne, F31062 Toulouse Cedex, France*

D. J. Wales

*University Chemical Laboratories, Cambridge CB2 1EW, United Kingdom*

Using approximate partition functions and a master equation approach, we investigate the statistical relaxation toward equilibrium in selected  $\text{CaAr}_n$  clusters. The Gaussian theory of absorption [J. Chem. Phys., **000**, 0000, 2003] is employed to calculate the average photoabsorption intensity associated with the  $4s^2 \rightarrow 4s^1 4p^1$  transition of calcium as a function of time during relaxation. In  $\text{CaAr}_6$  and  $\text{CaAr}_{10}$  simple relaxation is observed with a single time scale.  $\text{CaAr}_{13}$  exhibits much slower dynamics and the relaxation occurs over two distinct time scales.  $\text{CaAr}_{37}$  shows much slower relaxation with multiple transients, reminiscent of glassy behavior due to competition between different low-energy structures. We interpret these results in terms of the underlying potential energy surfaces for these clusters.

### I. INTRODUCTION

Clusters of van der Waals atoms or molecules are known to exhibit significant finite size effects<sup>1</sup> in their thermodynamic behavior. In particular, their structure and low-temperature stable phase can strongly depend on size. By doping such clusters with a chromophoric atom, spectroscopic techniques are able to characterize the structure of the whole complex. Very often, the chromophore only acts as a small perturbation on the geometry of the host van der Waals cluster, and spectroscopy can then be used as a probe of structure and structural changes in the cluster. These ideas, which date back to experimental studies in the eighties,<sup>2,3</sup> have received some theoretical support in the recent years.<sup>4,5</sup> In the previous paper in this series,<sup>6</sup> the influence of temperature and cluster size on the photoabsorption spectrum in  $\text{CaAr}_n$  clusters was investigated. In some cases, such as  $\text{CaAr}_{13}$  or  $\text{CaAr}_{37}$ , features in the absorption spectrum were seen to originate from the competition between specific isomers. These results were obtained using the quantum superposition method,<sup>7</sup> which yields ergodic data by construction from a database of local minima on the potential energy surface (PES).

However, the equilibrium properties computed from the superposition approach obviously provide no information about the way in which equilibrium was established, or how long equilibration would take from a given starting distribution. As was shown by Miller and coworkers,<sup>8</sup> relaxation can be rather slow when the competing minima are separated by large (free) energy barriers. In cases such as  $\text{Ar}_{38}$ , conventional molecular dynamics simulations are presently unable to reach equilibrium and thus cannot provide estimates of the rate constants. However, the master equation dynamics approach, introduced in cluster physics by Kunz and Berry,<sup>11</sup> has been successfully applied to this system,<sup>12</sup> although a subsequent discrete path sampling

study located somewhat faster pathways.<sup>14</sup> In particular, it has been used to calculate activation energies in the interconversion of  $(\text{NaCl})_{35}^-$  nanocrystals<sup>15</sup> that could be compared to those extracted from ion mobility measurements.<sup>13</sup>

It is important to characterize the dynamics of the  $\text{CaAr}_n$  clusters investigated previously at thermodynamical equilibrium, because the time required for reaching equilibrium may not always be accessible in experiments. In addition, the most powerful way to investigate phase changes through spectroscopy on single clusters may require ion trapping.<sup>35,36</sup> In principle, this technique can be used to examine the system over very long time scales, which makes it a possible tool for studying dynamics, including relaxation toward thermal equilibrium, possibly via kinetic traps.

This article is a natural extension to our previous work, and provides an investigation of the relaxation dynamics in some selected  $\text{CaAr}_n$  clusters, as evidenced by their photoabsorption spectra. In the next section, we briefly recall the basic ingredients of the master equation approach, and we incorporate quantum corrections to the equilibrium probabilities and rate constants. These corrections are necessary for consistency with the previous article.<sup>6</sup> Before actually studying dynamical processes, we construct and discuss disconnectivity graphs<sup>19,40</sup> in Sec. III. Such graphs are very helpful in elucidating the role of the underlying PES on the kinetics. Disconnectivity graphs are presented and discussed for the clusters  $\text{CaAr}_6$ ,  $\text{CaAr}_{10}$ ,  $\text{CaAr}_{13}$ , and  $\text{CaAr}_{37}$ , which were investigated in reference 6. Using the Gaussian theory of absorption inspired by Wadi and Pollak,<sup>6,16</sup> we calculate the photoabsorption intensity of these clusters as a function of both time and excitation energy. The results are given and analysed in Sec. IV, before we summarize and conclude in Sec. V.

## II. MASTER EQUATION DYNAMICS

In the master equation approach,<sup>17,18</sup> the interbasin dynamics on the energy landscape is described by the time evolution of a vector,  $\mathbf{P}(t)$ , whose components are the probabilities of the system residing in each of the basins at time  $t$ . The differential equations governing this evolution are

$$\frac{dP_i}{dt} = \sum_{j \neq i} [k_{ij}P_j(t) - k_{ji}P_i(t)], \quad (1)$$

where  $k_{ij}$  is the rate constant for transitions leading from minimum  $j$  to minimum  $i$ . A transition matrix  $\mathbf{W}$  is defined with components<sup>17,18,19</sup>

$$W_{ij} = k_{ij} - \delta_{ij} \sum_m k_{mi}, \quad (2)$$

and Eq. (1) is solved analytically after symmetrization and diagonalization of the matrix  $\mathbf{W}$ .<sup>18,19</sup> The rate constant  $k_{ij}$  is the sum over all transition states separating minima  $i$  and  $j$ :

$$k_{ij} = \sum_{\alpha} k_j^{\alpha}, \quad (3)$$

where  $k_j^{\alpha}$  is given by the usual Rice-Ramsperger-Kassel-Marcus theory.<sup>20,21,22,23,24,25</sup> In the canonical ensemble we have

$$k_j^{\alpha}(T) = \frac{k_B T}{2\pi\hbar} \frac{Z_j^{\alpha}(T)}{Z_j(T)}, \quad (4)$$

where  $k_B$  and  $h$  are Boltzmann's and Planck's constants, respectively.  $Z_j^{\alpha}$  and  $Z_j$  are the partition functions corresponding to the transition state  $\alpha$  between  $i$  and  $j$ , and to the minimum  $j$ , respectively. Here we use the harmonic approximation to model both  $Z_j^{\alpha}$  and  $Z_j$ , but we incorporate quantum corrections by employing the expressions for quantum oscillators:

$$Z_j(T) = \frac{h_j}{(2\pi)^{\nu} N!} e^{-\beta E_j} \prod_{k=1}^{\nu} \frac{\exp(-\beta\hbar\omega_{jk}/2)}{1 - \exp(-\beta\hbar\omega_{jk})}, \quad (5)$$

$$Z_j^{\alpha}(T) = \frac{h_j^{\alpha}}{(2\pi)^{\nu-1} N!} e^{-\beta E_j^{\alpha}} \prod_{k=1}^{\nu-1} \frac{\exp(-\beta\hbar\omega_{jk}^{\alpha}/2)}{1 - \exp(-\beta\hbar\omega_{jk}^{\alpha})}. \quad (6)$$

In these expressions,  $h_j$  (resp.  $h_j^{\alpha}$ ) denotes the order of the point group of minimum  $j$  (resp. transition state  $\alpha$  between minima  $i$  and  $j$ ).  $E_j$  and  $E_j^{\alpha}$  are the energy of these stationary points, and  $\{\omega_{jk}\}$  and  $\{\omega_{jk}^{\alpha}\}$  are their respective normal mode frequencies.  $\nu = 3N - 6$  is the number of independent degrees of freedom of the cluster, and  $\beta = 1/k_B T$ . In the limit  $\hbar \rightarrow 0$ , the rate constant tends to its usual classical value

$$k_j^{\alpha}(\hbar \rightarrow 0) = \frac{h_j^{\alpha}}{h_j} \frac{(\bar{\omega}_j)^{\nu}}{(\bar{\omega}_j^{\alpha})^{\nu-1}} e^{-\beta(E_j^{\alpha} - E_j)}, \quad (7)$$

where  $\bar{\omega}_j$  and  $\bar{\omega}_j^{\alpha}$  are the geometric mean normal mode frequencies of the minimum and transition state, respectively. In the low temperature limit  $\beta \rightarrow \infty$ , the rate is proportional to  $T \exp[-(E_j^{\alpha} - E_j^0)/k_B T]$ , where  $E_j^{\alpha 0}$  and  $E_j^0$  are the energies of the two stationary points including the zero-point energy contributions. While  $E_j^{\alpha} - E_j$  is always positive, it may well be that  $E_j^{\alpha 0} < E_j^0$ , leading to a divergent rate. In this case the two minima cannot be treated independently because of strong quantum delocalization effects. However, this situation should not arise at high or moderate temperatures where  $k_B T$  is large compared to the zero-point energy, and this is the regime of interest in the present work.

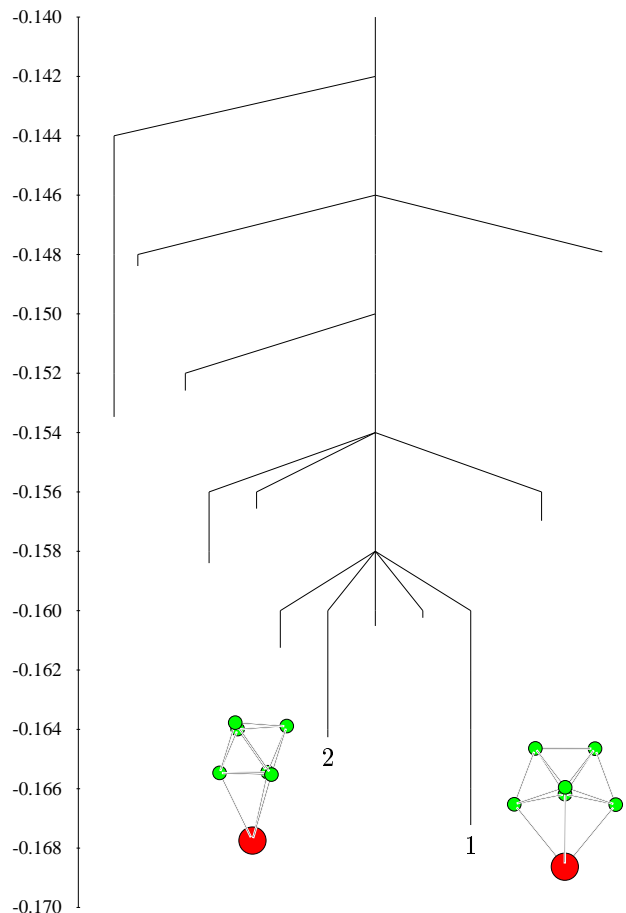


FIG. 1: Disconnectivity graph of the  $\text{CaAr}_6$  cluster. The energies are in eV.

Application of the master equation approach requires one to build a connected set of minima and the interwell transition states.<sup>19</sup> To do this we used eigenvector-following<sup>26</sup> in conjunction with several methods to sample the local minima.<sup>19</sup> For small clusters containing less than 11 atoms, systematic searches were started from the global minimum, and continued until no new minima were found after searching for transition states along every eigenvector of each minimum in the set. For these systems the connected set of minima should be nearly

complete. For  $\text{CaAr}_{13}$ , we expect the number of distinct local minima to be significantly larger than in  $\text{Ar}_{14}$ , which itself possesses more than  $10^4$ , excluding permutation-inversion isomers. We decided to perform only one cycle of systematic eigenvector-following transition state searches from each mode of every minimum in the database collected for the study at thermodynamic equilibrium.<sup>6</sup>

The situation becomes quite critical for  $\text{CaAr}_{37}$ . As was shown in our previous study,<sup>6</sup> several minima with different structures coexist at low energy, and we were not able to build a connected set containing all these minima using one systematic eigenvector-following cycle from the database obtained with parallel tempering Monte Carlo. For this larger cluster, we selected a small set of the low energy minima of interest, and we attempted to find discrete pathways (series of minima-transition states-minima) connecting them. To do this we followed the method described in reference 14, where a connected path is built up using successive double-ended pathway searches. The nudged-elastic-band approach<sup>27,28,29,30,31,32</sup> was used to generate initial guesses for transition states, which were then used as the starting points for hybrid eigenvector-following transition state searches<sup>33,34</sup>. These initial paths generally have rather high barriers, and so the discrete path sampling approach was then employed to provide a more realistic account of the rates.<sup>14</sup> These calculations also produce connected databases of minima and transition states that should provide a more appropriate picture of the dynamics, either in visualisations using disconnectivity graphs, or from master equation calculations. All the geometry optimisations and pathway calculations were performed with the OPTIM software package,<sup>19,37</sup> for which we implemented the pairwise potential describing the ground state potential energy surface of  $\text{CaAr}_n$  clusters.<sup>38</sup>

### III. ENERGY LANDSCAPES

A convenient way of visualizing complex energy landscape is to construct a disconnectivity graph. Such graphs were introduced by Becker and Karplus<sup>40</sup> in their study of a tetrapeptide. They have since been used in a much wider context.<sup>19</sup> Disconnectivity graphs show how the minima of the PES are connected to each other and, more importantly, what is the height of the barriers between these minima. Further details about the construction of disconnectivity graphs can be found in reference 19.

In the present work we have included zero-point energy corrections for the energies of the minima and transition states. Burnham *et al.* have previously found that zero-point effects change the appearance of disconnectivity graphs for the water hexamer significantly.<sup>41</sup> As noted in the previous section, the zero-point terms sometimes lead to the merging of two (and possibly more) minima. However, such events were not observed in  $\text{CaAr}_6$ , for

which we located twelve distinct minima and twenty transition states. The disconnectivity graph for this cluster is shown in Fig. 1 along with the two lowest energy isomers. According to the terminology introduced in reference 39, this graph has a typical ‘palm tree’ character: the global minimum lies at the bottom of a single funnel, and the absence of large energy barriers is expected to permit relatively fast relaxation toward equilibrium.

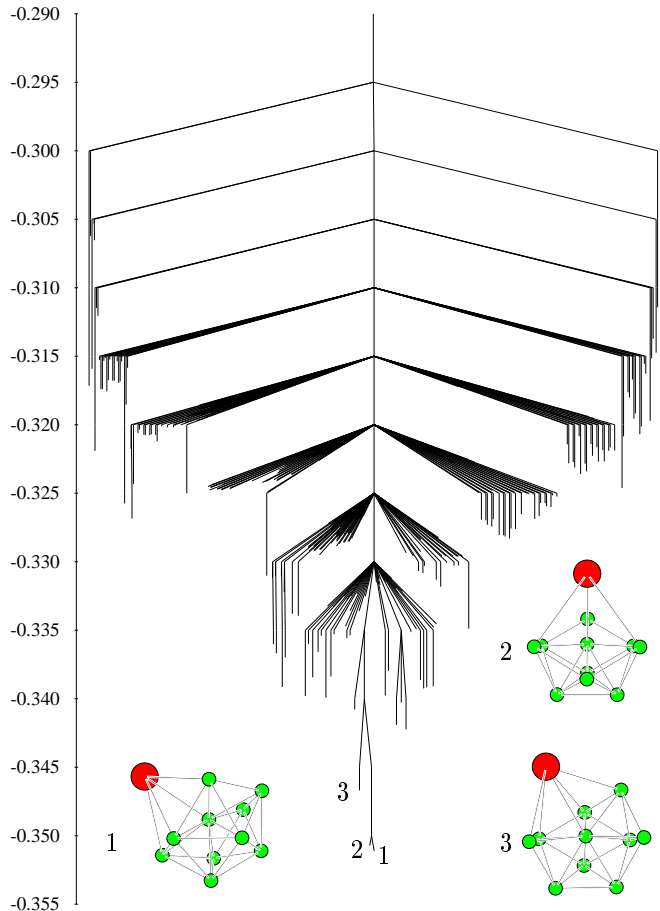


FIG. 2: Disconnectivity graph of the  $\text{CaAr}_{10}$  cluster. The energies are in eV.

A similar picture was found for the larger cluster,  $\text{CaAr}_{10}$ , as shown in Fig. 2. In this case we located 391 distinct minima connected via 1831 transition states. At the bottom of the funnel, the three lowest-energy minima lie close together. They are all based on the incomplete icosahedra, with different substitutional sites for the calcium atom. As Fig. 2 shows, the two lowest minima are extremely close in energy, and the energy barrier that separates them is very small (less than  $10^{-3}$  eV). Hence these two isomers can barely be considered distinct.

The disconnectivity graph of  $\text{CaAr}_{13}$  is shown in Fig. 3. The ‘palm tree’ character of this graph also suggests that relatively fast relaxation should be possible to the global minimum. However, the bottom of the funnel is slightly rugged due to the presence of additional isomers with respect to what would be expected for  $\text{Ar}_{14}$ . The four ex-

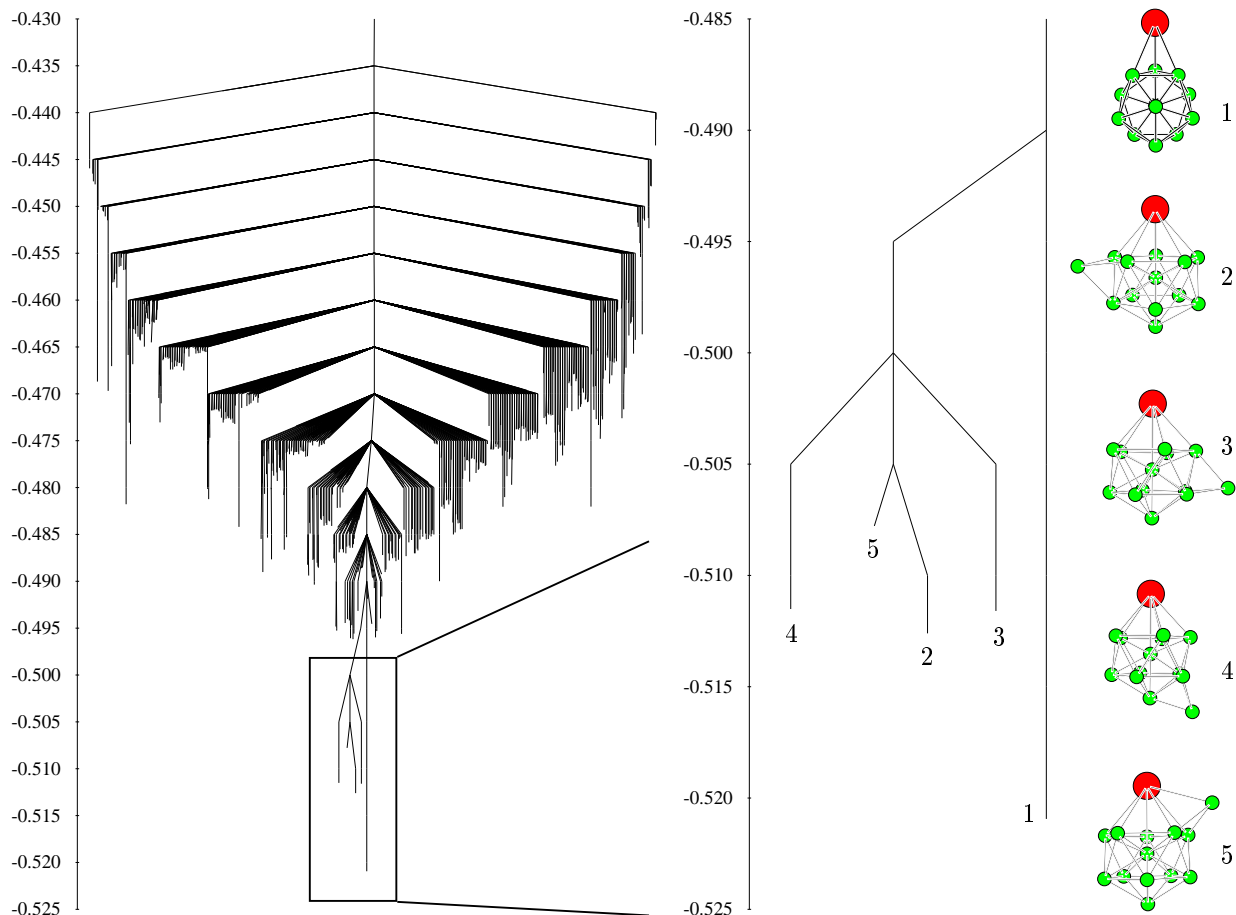


FIG. 3: Disconnectivity graph of the  $\text{CaAr}_{13}$  cluster. The right panel shows the lower part of the graph and the secondary funnel associated to changing the substitutional site of calcium in the capped icosahedron structure. All energies are in eV.

tra structures found by changing the substitutional site of the calcium atom create a secondary side funnel. They are close in energy to the global minimum, and are displayed in Fig. 3 next to a more detailed view of the corresponding part of the graph. The ordering between these isomers is straightforwardly explained by the weaker Ca–Ar bond compared to  $\text{Ar}_2$ . The lowest-energy barrier between the global minimum and the next four isomers lies about  $2.19 \times 10^{-3}$  eV/atom above isomer 1, which is equivalent to a temperature of about 25 K. Below this temperature we expect the relaxation to the global minimum to become significantly slower due to trapping in the secondary funnel.

Finally we consider the larger  $\text{CaAr}_{37}$  cluster. Starting from the ten lowest minima in the database obtained by systematic quenching along a parallel tempering Monte Carlo trajectory,<sup>6</sup> we were able to establish twenty connected discrete pathways using the method described in reference 14. New low-energy minima were discovered, two of them lower than some in the initial set. Four additional pathways were then constructed in the same way. As mentioned above, these initial pathways found may be far from optimal in terms of rates. The typical initial path contained 30–40 minima and the disconnec-

tivity graph constructed just from the initial pathway searches contained 731 distinct minima and 820 transition states. It is shown in Fig. 4, together with a selection of low-energy structures chosen from the initial sample. Clearly this graph does not show the single funnel aspect of the previous clusters, and resembles more the ‘banyan tree’ form.<sup>39</sup>

In fact, the energy landscape of  $\text{CaAr}_{37}$  is more complicated than that of  $\text{Ar}_{38}$ , which only has two main funnels associated with truncated octahedral or icosahedral structures, respectively. It is closer to the actual multiple funnel shape of the disconnectivity graph in the ionic cluster  $(\text{NaCl})_{35}$ .<sup>42</sup> This increased complexity is due to the larger number of isomers and possible binding sites for calcium, and to the existence of a particularly stable decahedral isomer. The stabilization of the anti-Mackay icosahedral structures (isomer 4) due to zero-point effects is another complicating factor.<sup>7</sup>

The  $\text{CaAr}_{37}$  cluster exhibits several similarities with  $\text{Ar}_{38}$ , such as the nonicosahedral global minimum and the multiple-funnel energy landscape. In thermal equilibrium, the low-temperature behavior is essentially governed by the decahedral and Mackay-type icosahedral minima.<sup>6</sup> The truncated octahedral isomer is not ex-

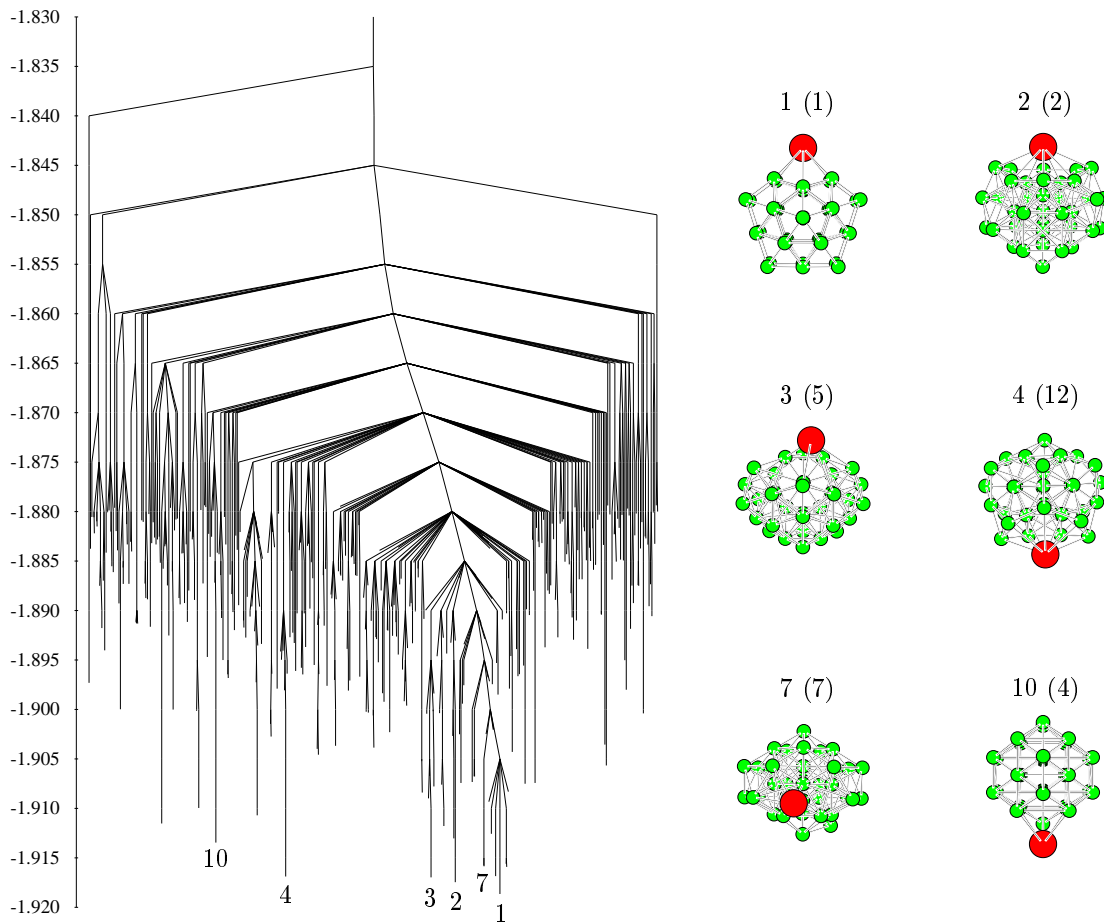


FIG. 4: Disconnectivity graph of the  $\text{CaAr}_{37}$  cluster. Some isomers are represented on the right side of the graph, with their rank in the quantum (classical) regime. The energies are in eV.

pected to play a major role in the relaxation dynamics, except if it contributes significantly to the initial conditions.

From Fig. 4 we see that the decahedral and Mackay icosahedra isomers belong to the same superbasin at relatively low energies. Hence we expect to find significantly faster relaxation than in  $\text{Ar}_{38}$ , where the truncated octahedron and the icosahedra are much farther apart in configuration space, and separated by a relatively high barrier. However, to obtain insight into the relative stabilities of the isomers at the temperature where relaxation is simulated, it may be helpful to include entropic effects in the disconnectivity graphs.<sup>43,44</sup> To achieve this goal we simply computed the free energies of the minima and transition states instead of potential energy minima, replacing  $E_j$  ( $E_j^\alpha$ ) by  $F_j = -k_B T \ln Z_j$  ( $F_j^\alpha = -k_B T \ln Z_j^\alpha$ ), where the partition functions were obtained in the harmonic approximation, and taken from Eqn. (5,6).

The free-energy disconnectivity graph of  $\text{CaAr}_{37}$  at  $T = 20\text{ K}$  is represented in Fig. 5. As can be clearly seen on this figure, the most stable minimum at this temperature is the anti-Mackay icosahedron isomer (4), and the free energy barrier to the decahedral and Mackay-

icosahedral minima seems rather large. This change in the most stable funnel with respect to the  $T = 0$  disconnectivity graph should hinder relaxation, and we therefore anticipate particularly slow dynamics.

#### IV. RELAXATION TO EQUILIBRIUM: TIME-DEPENDENT ABSORPTION SPECTRA

We now turn to the relaxation properties of  $\text{CaAr}_n$  clusters resulting from the solution of the master equation. Two types of relaxation have been considered, either starting from  $T = 0$  (only the quantum global minimum is occupied) and moving to higher  $T$ , or starting from a finite temperature equilibrium distribution and changing to lower  $T$ . The equilibrium distributions were calculated within the quantum harmonic superposition approach applied to the same database of minima that was used to construct the disconnectivity graphs, without reweighting. For  $\text{CaAr}_{37}$ , this procedure yields a heat capacity peak corresponding to melting located at about 25 K, slightly higher than the one obtained in the more thorough previous study.<sup>6</sup> For the other clusters the harmonic approximation without reweighting performs

rather well.

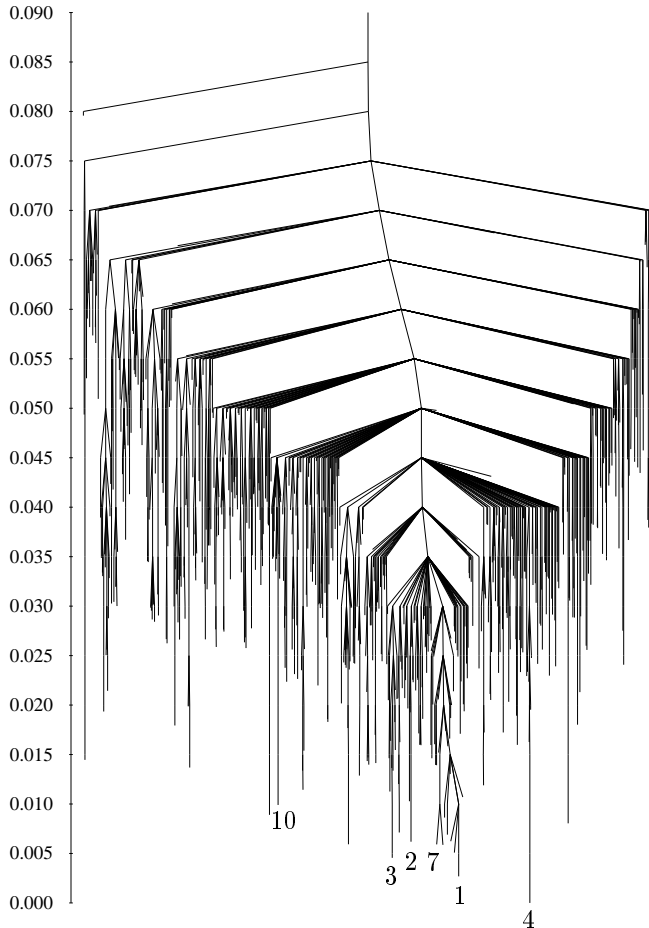


FIG. 5: Free-energy disconnectivity graph of the  $\text{CaAr}_{37}$  cluster, calculated at  $T = 20$  K using harmonic quantum partition functions. The isomers of Fig. 4 are represented. The energies relative to the lowest free-energy minimum are in eV.

Here we focus on the photoabsorption spectrum as a possible probe of cluster structure in a dynamical context. The absorption intensity of the  $4s^2 \rightarrow 4s^1 4p^1$  excitation for calcium was calculated using the Gaussian theory adapted and extended from the work of Wadi and Pollak.<sup>6,16</sup> The excited state potential energy surfaces were modelled by a diatomics-in-molecules (DIM) Hamiltonian, which was fully described in Ref. 38.

We first show in Fig. 6 the time evolution of the absorption spectrum of  $\text{CaAr}_6$ , starting at  $t = 0$  from the zero temperature distribution, and relaxing at  $T = 25$  K, slightly above the melting point.<sup>6</sup> The spectrum remains essentially doubly-peaked, and at very small times  $t < 5$  ps the red peak can be separated into two distinct lines characteristic of the ground state isomer. The blue wing of this peak soon becomes a shoulder. These results correspond to fast relaxation, which barely has a spectroscopic signature. Such simple dynamics is perfectly consistent with the energy landscape of this cluster, as seen from its disconnectivity graph. In the upper panel of Fig. 6, the characteristic time constants,  $\tau_i$ , of the rate

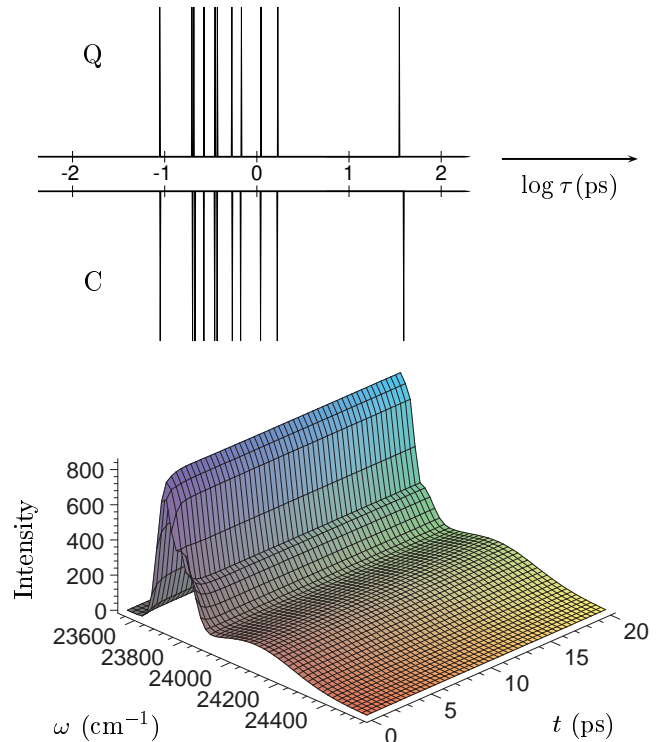


FIG. 6: Photoabsorption spectrum of  $\text{CaAr}_6$  during the relaxation from the  $T = 0$  distribution toward the  $T = 25$  K equilibrium distribution. The discrete spectra [in the quantum (Q) and classical (C) regimes] of the characteristic times of the transition matrix  $\mathbf{W}$  are represented on a decimal logarithmic scale, on the horizontal axis in the upper part of the figure.

matrix  $\mathbf{W}$  are represented on a horizontal axis, for both the quantum and classical regimes. They are calculated from the nonzero eigenvalues,  $\lambda_i$ , of  $\mathbf{W}$  as  $\tau_i = -1/\lambda_i$ . At 25 K, the largest time constant is a few tens of picoseconds, which is roughly in agreement with the observed decay of the spectroscopic signal, although the experimental relaxation is faster, by about one order of magnitude, than the slowest time constant  $\tau_{\text{max}}$ . Such quantitative discrepancies are typical of the errors that simple rate theories based upon harmonic densities of states are expected to introduce. Quantum effects are small in this system and the relaxation kinetics for  $\text{CaAr}_{10}$  were found to be very similar, so detailed discussion is omitted.

Relaxation from a zero temperature distribution has also been investigated in  $\text{CaAr}_{13}$  for a temperature jump to  $T = 40$  K, which lies close to the melting point of this cluster.<sup>6</sup> At this temperature, the occupation probability of the secondary funnel is quite large. The time-dependent spectrum in Fig. 7 indeed exhibits a transition from the ground state, identified by two absorption peaks, to vibrationally excited isomers and the three-peak pattern characteristic of calcium located in the icosahedral shell.<sup>6</sup> Monitoring the time-dependent signal



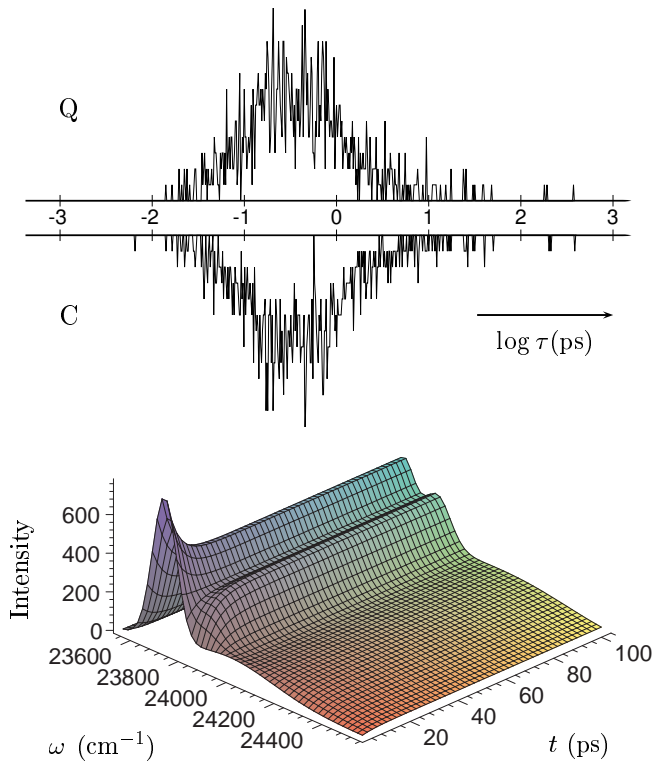


FIG. 7: Photoabsorption spectrum of  $\text{CaAr}_{13}$  during the relaxation from the  $T = 0$  distribution toward the  $T = 40$  K equilibrium distribution. The continuous distributions [in the quantum (Q) and classical (C) regimes] of the characteristic times of the transition matrix  $\mathbf{W}$  are represented on a decimal logarithmic scale, on the horizontal axis in the upper part of the figure.

shows that relaxation typically occurs on a 50 ps time scale, which is again one order of magnitude faster than  $\tau_{\text{max}}$  in this system, as seen in the upper part of Fig. 7.

At  $T = 20$  K, the global minimum of  $\text{CaAr}_{13}$  is predicted to have an equilibrium occupation probability larger than 90%,<sup>6</sup> hence the next metastable isomers play only a minor role in the thermodynamic properties. Relaxation from a high temperature distribution (50 K) has also been simulated using the master equation approach. The time-dependent absorption spectrum is plotted in Fig. 8 along with the distribution of characteristic decay times from the rate matrix. The variations observed in the spectrum are in clear contrast with the previous results. During the first 100 ps, the cluster relaxes from a broad distribution of isomers towards the main funnel that corresponds to the capped icosahedron. As indicated by the two-peak absorption spectrum, the secondary funnel has a larger occupation probability about 5 ns after the dynamics has started. The cluster then finally relaxes to its equilibrium distribution following single exponential kinetics, characterized by a rather large time constant of about  $10^5$  ps. This value is still one order of magnitude faster than the calculated  $\tau_{\text{max}} \approx 10^6$  ps,

represented in the upper part of Fig. 8. The two-step relaxation process observed here can be easily interpreted thanks to the disconnectivity graph in Fig. 3. The secondary funnel constitutes a kinetic trap, resulting in a significant slowing down of the dynamics. While the cluster easily finds its way into this secondary funnel, escape to the global minimum is much slower due to the rather large energy barrier. In agreement with previous work, this multiple-funnel landscape exhibits a separation of timescales in its dynamics.<sup>19,39</sup>

We finally discuss the case of  $\text{CaAr}_{37}$ , for which we solved the master equation at  $T = 20$  K, starting from the  $T = 0$  initial distribution. The magnitude of the characteristic decay times, as computed from the eigenvalues of the rate matrix, are remarkably large, reaching values close to one second. The calculated absorption spectrum is shown in Fig. 9 as a function of time. The choice of a logarithmic scale emphasizes the different time scales present in this system. The multiple funnels of the energy landscape are in competition below 20 K, and the cluster undergoes multiple transitions before reaching equilibrium. As we deduced from the free energy disconnectivity graph in Fig. 5, relaxation from 0 to 20 K in this system requires the cluster to escape from its initial decahedral/icosahedral funnel. At least four significant changes in behaviour are detected through absorption spectroscopy, after  $10^2$ ,  $10^6$ ,  $10^{10}$ , and  $10^{12}$  ps, respectively. The transient regime thus appears particularly slow, in a similar way to the dynamics observed in  $\text{Ar}_{38}$ .<sup>8</sup> The spectra in Fig. 9 show that some intermediate minima, which are too high in energy to be significantly occupied at equilibrium, may still contribute to the spectrum as transient species with a long lifetime.

For  $\text{CaAr}_{37}$  the set of connected minima was initially constructed in a rather artificial manner by means of direct pathway searches. As mentioned in the previous section, these initial paths are usually rather long and correspond to high barriers. Therefore the interconversion rates predicted using this database are probably unrealistic and much too low. The discrete path sampling technique<sup>14</sup> was therefore used to optimize the pathway between the two lowest decahedral and Mackay icosahedral minima. We found pathways containing fewer than seven minima (including the two end points) with a rate constant about eight orders of magnitude larger than that of the initial 45-step pathway. This improvement is even more impressive than the one found for  $\text{Ar}_{38}$ .<sup>14</sup> However, in  $\text{CaAr}_{37}$  the distance between the two minima in question is rather shorter, because they belong to the same funnel.

We did not attempt to optimize the 23 other initial pathways using the discrete path sampling method, since the effect of refining the interconversion pathways is not expected to affect the complex variation with time of the absorption intensity.

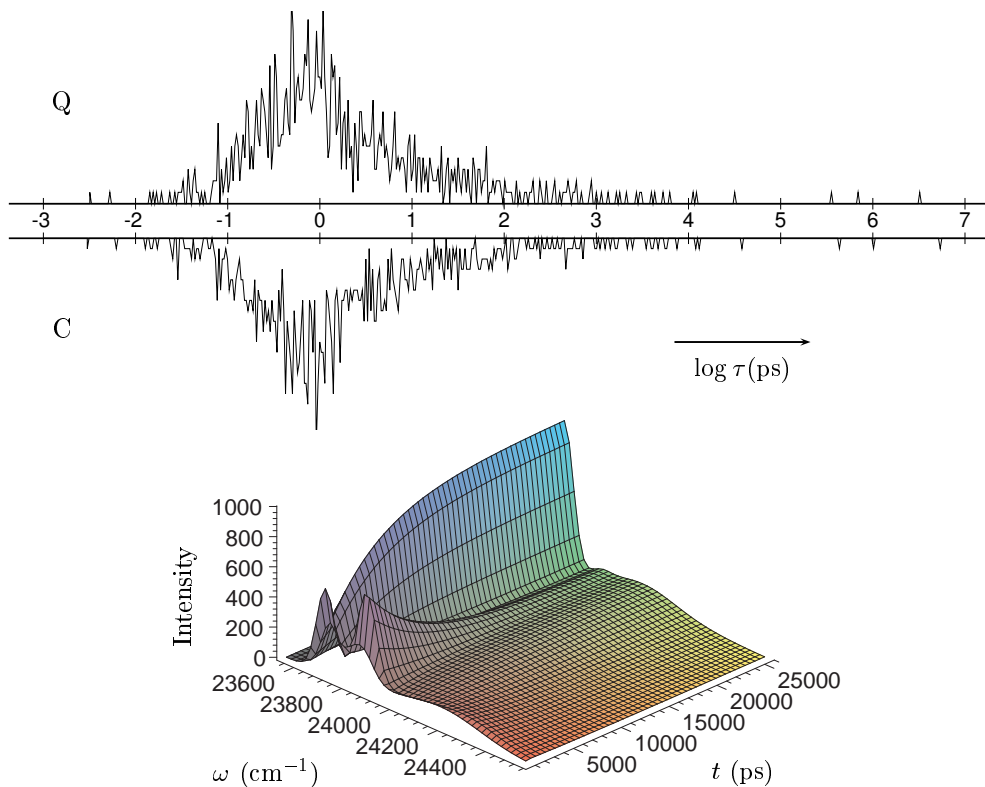


FIG. 8: Photoabsorption spectrum of  $\text{CaAr}_{13}$  during the relaxation from the  $T = 50$  distribution toward the  $T = 20$  K equilibrium distribution. The continuous distributions [in the quantum (Q) and classical (C) regimes] of the characteristic times of the transition matrix  $\mathbf{W}$  are represented on a decimal logarithmic scale, on the horizontal axis in the upper part of the figure.

## V. CONCLUSIONS

The complexity of the energy landscapes of  $\text{CaAr}_n$  clusters is reflected not only on their equilibrium properties, but also in their relaxation kinetics. By employing the master equation approach, quantum corrected harmonic partition functions and the Gaussian theory of absorption,<sup>16</sup> we have investigated the time-dependence of the photoabsorption intensity. The clusters were chosen to provide a selection of various finite-size effects. Our main result is that spectroscopy may be able to probe the isomerization of a given cluster in real time, and provide estimates of the interconversion rates themselves. We have found evidence that  $\text{CaAr}_n$  clusters can display simple kinetics (as in  $\text{CaAr}_6$  or  $\text{CaAr}_{10}$ ), two-state kinetics and trapping in auxiliary funnels ( $\text{aAr}_{13}$ ), or more intricate kinetics and multiple transient regimes ( $\text{CaAr}_{37}$ ), all with a distinct spectroscopic signature. ex-

periments?

A number of approximations have been used to achieve these results, including the harmonic superposition approximation using incomplete samples of minima for the larger clusters. The master equation approach also contains some assumptions, such as local equilibrium inside each basin and Markovian dynamics. Finally, the Gaussian theory of absorption also contains some approximations. Because of these restrictions, our investigation may be semi-quantitative with respect to actual  $\text{CaAr}_n$  clusters, even before we allow for the approximate nature of the Hamiltonians used to model the ground- and excited-state potential energy surfaces.<sup>38</sup> Nevertheless, the present study provides the next step beyond the analysis of equilibrium properties discussed in our previous paper.<sup>6</sup> We believe that it further supports the need for future experiments on size-selected, trapped clusters studied via spectroscopic techniques.

<sup>1</sup> J. Jortner, *Z. Phys. D* **24**, 247 (1992).

<sup>2</sup> M. Y. Hahn and R. L. Whetten, *Phys. Rev. Lett.* **61**, 1190 (1988).

<sup>3</sup> U. Even, N. Ben-Horin, and J. Jortner, *Phys. Rev. Lett.* **62**, 140 (1989).

<sup>4</sup> M. R. Ghayal and E. Curotto, *J. Chem. Phys.* **111**, 5522 (1999).

<sup>5</sup> M. Moseler, H. Hakkinen, and U. Landman, *Phys. Rev. Lett.* **87**, 053401 (2001).

<sup>6</sup> F. Calvo, F. Spiegelman, and M.-C. Heitz, previous article.



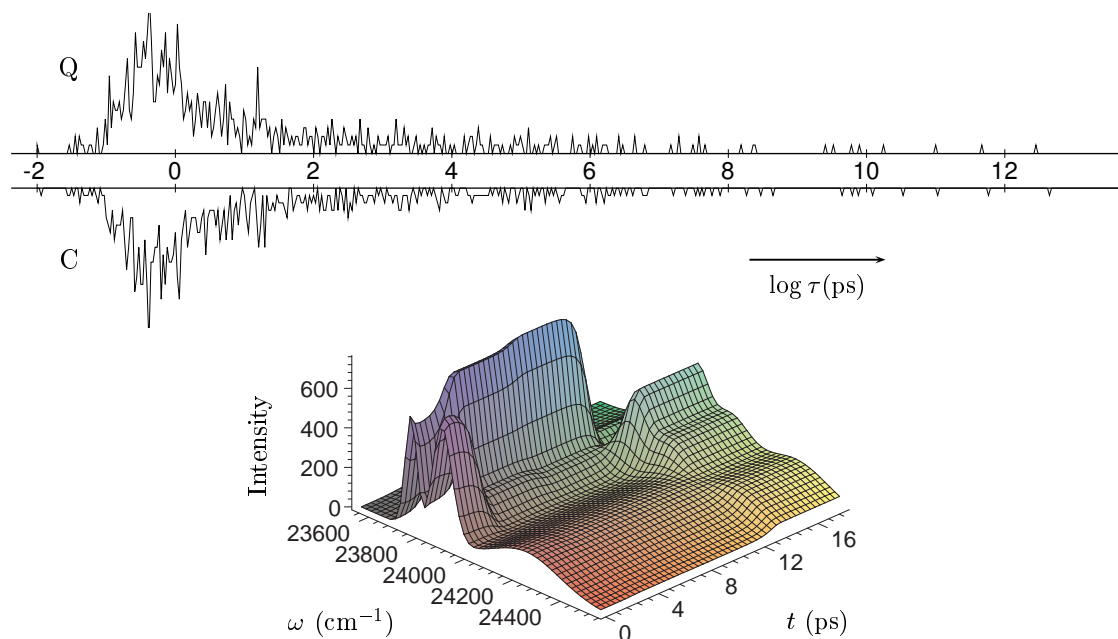


FIG. 9: Photoabsorption spectrum of  $\text{CaAr}_{37}$  during the relaxation from the  $T = 0$  distribution toward the  $T = 20$  K equilibrium distribution. The continuous distributions [in the quantum (Q) and classical (C) regimes] of the characteristic times of the transition matrix  $\mathbf{W}$  are represented on a decimal logarithmic scale, on the horizontal axis in the upper part of the figure.

- <sup>7</sup> F. Calvo, J. P. K. Doye, and D. J. Wales, *J. Chem. Phys.* **114**, 7312 (2001).
- <sup>8</sup> M. A. Miller, J. P. K. Doye, and D. J. Wales, *Phys. Rev. E* **60**, 3701 (1999).
- <sup>9</sup> A. F. Voter, *J. Chem. Phys.* **106**, 4665 (1997).
- <sup>10</sup> P. G. Bolhuis, D. Chandler, C. Dellago, and P. L. Geissler, *Annu. Rev. Phys. Chem.* **53**, 291 (2002).
- <sup>11</sup> R. E. Kunz and R. S. Berry, *Phys. Rev. Lett.* **74**, 3951 (1995); *J. Chem. Phys.* **103**, 1904 (1995).
- <sup>12</sup> J. P. K. Doye, M. A. Miller and D. J. Wales, *J. Chem. Phys.* **110**, 6896 (1999).
- <sup>13</sup> R. R. Hudgins, P. Dugourd, J. M. Tenenbaum, and M. F. Jarrold, *Phys. Rev. Lett.* **78**, 4213 (1997).
- <sup>14</sup> D. J. Wales, *Mol. Phys.* **100**, 3285 (2002).
- <sup>15</sup> J. P. K. Doye and D. J. Wales, *J. Chem. Phys.* **111**, 11070 (1999).
- <sup>16</sup> H. Wadi and E. Pollak, *J. Chem. Phys.* **110**, 11890 (1999).
- <sup>17</sup> N. G. van Kampen, *Stochastic Processes in Physics and Chemistry* (North-Holland, Amsterdam, 1981).
- <sup>18</sup> R. E. Kunz, *Dynamics of First-Order Phase Transitions*, (Deutsch, Thun, 1995).
- <sup>19</sup> D. J. Wales, J. P. K. Doye, M. A. Miller, P. N. Mortenson, and T. R. Walsh, *Adv. Chem. Phys.* **115**, 1 (2000).
- <sup>20</sup> O. K. Rice and H. C. Ramsperger, *J. Am. Chem. Soc.* **49**, 1616 (1927).
- <sup>21</sup> O. K. Rice and H. C. Ramsperger, *J. Am. Chem. Soc.* **50**, 617 (1928).
- <sup>22</sup> L. S. Kassel, *J. Phys. Chem.* **32**, 225 (1928).
- <sup>23</sup> R. A. Marcus, *J. Chem. Phys.* **20**, 359 (1952).
- <sup>24</sup> G. M. Wieder and R. A. Marcus, *J. Chem. Phys.* **37**, 1835 (1962).
- <sup>25</sup> R. A. Marcus, *J. Chem. Phys.* **43**, 2658 (1965).
- <sup>26</sup> C. J. Cerjan and W. H. Miller, *J. Chem. Phys.* **75**, 2800 (1981).
- <sup>27</sup> G. Mills and H. Jónsson, *Phys. Rev. Lett.* **72**, 1124 (1994).
- <sup>28</sup> H. Jónsson, G. Mills and K. W. Jacobsen, in *Classical and Quantum Dynamics in Condensed Phase Simulations*, edited by B. J. Berne, G. Ciccotti and D. F. Coker, World Scientific, Singapore (1998).
- <sup>29</sup> G. Henkelman, B. P. Uberuaga and H. Jónsson, *J. Chem. Phys.* **113**, 9901 (2000).
- <sup>30</sup> G. Henkelman and H. Jónsson, *J. Chem. Phys.* **113**, 9978 (2000).
- <sup>31</sup> G. Henkelman and H. Jónsson, *J. Chem. Phys.* **115**, 9657 (2001).
- <sup>32</sup> P. Maragakis, S. A. Andreev, Y. Brumer, D. R. Reichman and E. Kaxiras, *J. Chem. Phys.* **117**, 4651 (2002).
- <sup>33</sup> L. J. Munro and D. J. Wales, *Phys. Rev. B* **59**, 3969 (1999).
- <sup>34</sup> Y. Kumeda, L. J. Munro and D. J. Wales, *Chem. Phys. Lett.* **341**, 185 (2001).
- <sup>35</sup> M. Maier-Borst, D. B. Cameron, M. Rokni, and J. H. Parks, *Phys. Rev. A* **59**, R3162 (1999).
- <sup>36</sup> S. Kruckeberg, D. Schooss, M. Maier-Borst and J. H. Parks, *Phys. Rev. Lett.* **85**, 4494 (2000).
- <sup>37</sup> D. J. Wales, *OPTIM: A program for optimizing geometries and calculating reaction pathways*, Version 2.3 (University of Cambridge, Cambridge, 2002).
- <sup>38</sup> M. A. Gaveau, M. Briant, P. R. Fournier, J. M. Mestdagh, J. P. Visticot, F. Calvo, S. Baudrand, and F. Spiegelman, *Euro. Phys. J. D* **21**, 153 (2002).

- <sup>39</sup> D. J. Wales, M. A. Miller, and T. R. Walsh, *Nature (London)* **394**, 758 (1998).
- <sup>40</sup> O. M. Becker and M. Karplus, *J. Chem. Phys.* **106**, 1495 (1997).
- <sup>41</sup> C. J. Burnham, S. S. Xantheas, M. A. Miller, B. E. Applegate and R. E. Miller, *J. Chem. Phys.* **117**, 1109 (2002).
- <sup>42</sup> J. P. K. Doye and D. J. Wales, *Phys. Rev. B* **59**, 2292 (1999).
- <sup>43</sup> S. Krivov and M. Karplus, *J. Chem. Phys.* **117**, 10894 (2002).
- <sup>44</sup> D. A. Evans and D. J. Wales, *J. Chem. Phys.* **000**, 0000 (2003).